iScience

CellPress

Article

Activation of Hypoxia-Inducible Factor Signaling Modulates the RNA Protein Interactome in *Caenorhabditis elegans*

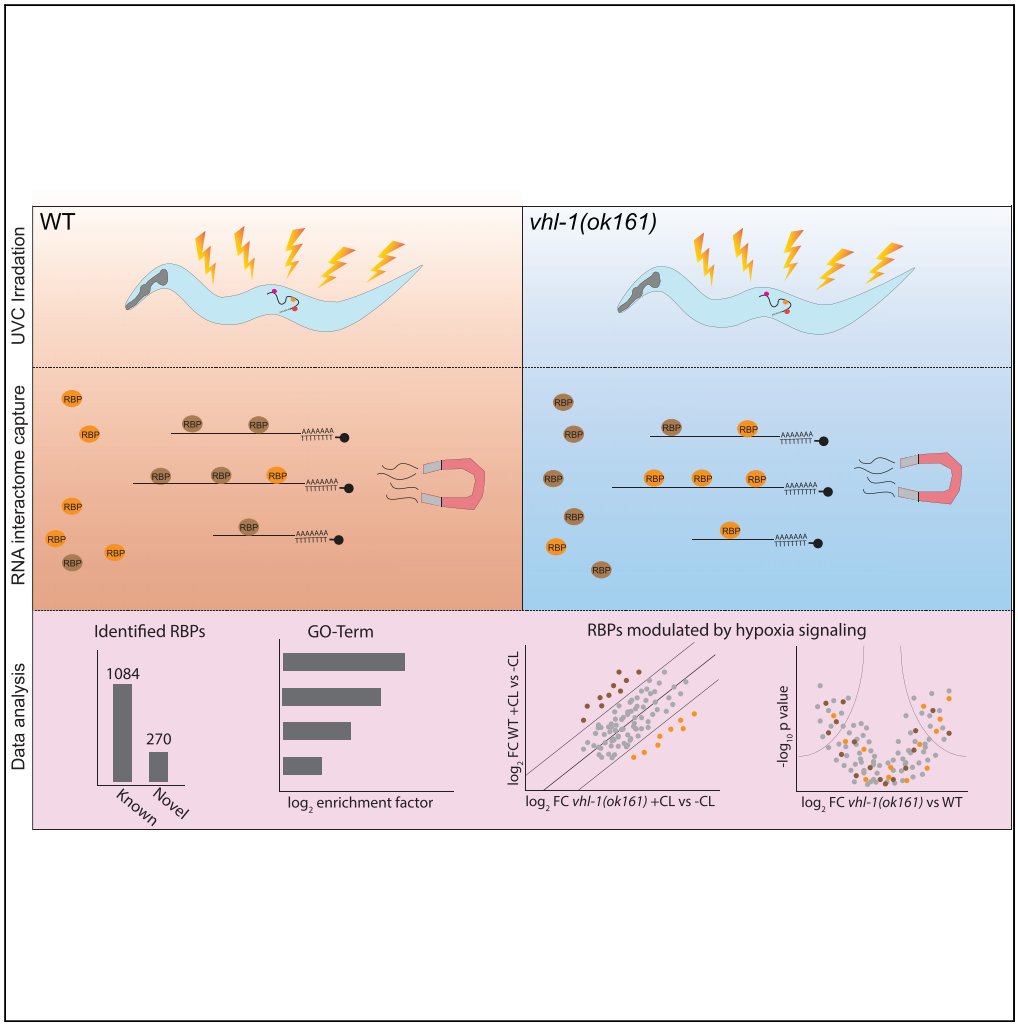

Reza Esmaillie, Michael Ignarski, Katrin Bohl, ..., Thomas Benzing, Roman-Ulrich Müller, Francesca Fabretti

roman-ulrich.mueller@uk-koeln.de

HIGHLIGHTS

RNA interactome capture in wild-type *C. elegans* and *vhl-1* loss-of-function mutants

Identification of 1,354 nematode RBPs, 270 of which can be considered novel RBPs

The modulation of the RBPome by *vhl-1* is primary explained by differential RNA-binding

The resulting RBP atlas is provided as an interactive online data mining tool

DATA AND CODE AVAILABILITY

PXD014469

Esmaillie et al., iScience *22*, 466–476
December 20, 2019
https://doi.org/10.1016/j.isci.2019.11.039

iScience

CellPress

Article

Activation of Hypoxia-Inducible Factor Signaling Modulates the RNA Protein Interactome in *Caenorhabditis elegans*

Reza Esmaillie,[1,2] Michael Ignarski,[1,2] Katrin Bohl,[1,2] Tim Krüger,[1,2] Daniyal Ahmad,[1,2] Lisa Seufert,[1,2] Bernhard Schermer,[1,2,3] Thomas Benzing,[1,2,3] Roman-Ulrich Müller,[1,2,3,4,5,*] and Francesca Fabretti[1,2,4]

SUMMARY

The cellular response to hypoxia is crucial to organismal survival, and hypoxia-inducible factors (HIF) are the key mediators of this response. HIF-signaling is central to many human diseases and mediates longevity in the nematode. Despite the rapidly increasing knowledge on RNA-binding proteins (RBPs), little is known about their contribution to hypoxia-induced cellular adaptation. We used RNA interactome capture (RIC) in wild-type *Caenorhabditis elegans* and *vhl-1* loss-of-function mutants to fill this gap. This approach identifies more than 1,300 nematode RBPs, 270 of which can be considered novel RBPs. Interestingly, loss of *vhl-1* modulates the RBPome. This difference is not primarily explained by protein abundance suggesting differential RNA-binding. Taken together, our study provides a global view on the nematode RBPome and proteome as well as their modulation by HIF-signaling. The resulting RBP atlas is also provided as an interactive online data mining tool (http://shiny.cecad.uni-koeln.de:3838/celegans_rbpome).

INTRODUCTION

RNA-binding proteins (RBPs) play an important role in cell biology, regulating expression, stability, and localization of all known RNA species (Halbeisen et al., 2008; Hasan et al., 2014; Lee and Lykke-Andersen, 2013; Wilkie et al., 2003). The importance of these proteins is underlined by the increasing body of evidence linking several hereditary diseases, developmental disorders, and cancer with mutations in genes encoding RBPs (Fredericks et al., 2015; Kechavarzi and Janga, 2014; Lukong et al., 2008). By using sequence motifs, many RBPs could be predicted by their classical RNA-binding domain (RBD)—e.g. RRM, ZINC finger domain, or PUF domain—and studied individually (Hall, 2005; Query et al., 1989; Zhang et al., 1997). However, their global characterization became possible only in the last years and was facilitated by novel techniques such as RNA interactome capture (RIC) combined with mass spectrometry to identify proteins co-precipitating with RNA (Baltz et al., 2012; Castello et al., 2012). As a result, the list of known and putative RBPs has been increasing in size and complexity across species with more than 2,000 proteins showing an interaction with RNA (Hentze et al., 2018). Interestingly, a significant number of these proteins lack classical RBDs—a finding that was the basis to the term enigmRBPs (Beckmann et al., 2015), showing that mere prediction by amino acid sequence and domain is not sufficient for an exhaustive identification of proteins capable of RNA binding. RBPs can be regulated not only on the level of protein abundance but also by modulation of their association with RNA, e.g. through differential RNA-binding capacity of the protein itself or availability of the actual RNA interaction partners. Consequently, the comparison of different environmental conditions and genetic mutants is crucial to gain a better understanding of the RBPome landscape (Jiang et al., 2014). As an example, this aspect was addressed regarding the induction of apoptosis in the only *Caenorhabditis elegans* (*C. elegans*) RIC dataset published to date (Matia-Gonzalez et al., 2015). In cell culture, a recent study from our group found differences in RBP-binding to RNA upon exposure to hypoxia (Ignarski et al., 2019). Key genes involved in sensing hypoxia are the hypoxia-inducible transcription factors (HIFs). HIF-1 is a heterodimer composed of an oxygen-sensitive α subunit and a constitutively expressed β subunit. HIF-1α is regulated by oxygen-dependent proline hydroxylation. Upon hydroxylation of HIF-1α, pVHL as the substrate recognition subunit of an E3 ubiquitin ligase binds to HIF-1α resulting in its proteasomal degradation. Upon hypoxia the HIF-1α subunit gets stabilized and translocates to the nucleus where it can exert its transcriptional activity as a heterodimeric transcription factor (Kaelin, 2005; Luo et al., 2014). Stabilization of HIF-1α can also be gained by a loss-of-function of the *VHL* gene, which is the basis to von Hippel-Lindau disease, an autosomal-dominant multitumor syndrome

[1]Department II of Internal Medicine and Center for Molecular Medicine Cologne, University of Cologne, Faculty of Medicine and University Hospital of Cologne, Cologne 50937, Germany

[2]Cologne Excellence Cluster on Cellular Stress Responses in Aging-associated Diseases (CECAD), University of Cologne, Cologne 50931, Germany

[3]Systems Biology of Ageing Cologne, University of Cologne, Cologne 50931, Germany

[4]These authors contributed equally

[5]Lead Contact

*Correspondence: roman-ulrich.mueller@uk-koeln.de

https://doi.org/10.1016/j.isci.2019.11.039

(Maxwell et al., 1999). A small number of studies have shown a potential role of specific RBPs on HIF-signaling (Cho et al., 2015; Galban et al., 2008). Yet, the global impact and regulation of RBPs in this pathway has not been sufficiently delineated. HIF-signaling and its regulation through pVHL are highly conserved with activation of HIF mediating longevity in nematodes (Mehta et al., 2009; Muller et al., 2009). Consequently, we chose this model organism to examine the impact of genetic activation of HIF-signaling on the RBP landscape to complement previous data at organismal level. In the study at hand, we performed RIC in wild-type (WT) and *vhl-1*(*ok161*) (from now on referred to as *vhl-1*) loss-of-function worms. We identified more than 1,000 bona-fide RBPs in WT and compared these results with *vhl-1* mutants to identify hypoxia-signaling induced changes in the nematode RBPome. This analysis was then combined with the whole proteome quantification in both nematode strains to distinguish changes in RBP abundance from differential binding events. An interactive online interface to visualize and interrogate these datasets is provided at http://shiny.cecad.uni-koeln.de:3838/celegans_rbpome. Taken together, our study provides the first global atlas of HIF-signaling-induced changes in the nematode RBPome.

RESULTS

Global Analysis of RBPs in WT and *vhl-1* Mutant Worms

We performed RIC using UV-C crosslinking and oligo(dT)-bead-based RNA pulldown coupled with mass spectrometry (MS) to obtain a global view on the nematode RBPome in WT and *vhl-1* mutant worms (Figure 1A). Protein concentration measurements of lysates obtained from 500 worms in both strains revealed a significantly lower protein yield in the *vhl-1* mutant strain (Figure S1A). In line with this result, the RNA concentration obtained from 500 worms from both strains also showed a significantly lower RNA yield in the *vhl-1* mutant strain (Figure S1B). In order to rule out that this would influence the results of the RIC we also measured the RNA concentration upon pooling the three eluates resulting from oligo(dT)-bead-based pulldown. These measurements revealed a similar amount in both strains and conditions (crosslinked and non-crosslinked) (Figure S1C). As expected, a higher amount of protein was co-precipitated in crosslinked samples from both strains (compared with the non-crosslinked samples) as shown by SDS-PAGE and silver staining (Figure 1B). The samples were then analyzed by MS. Principal component analysis (PCA) and hierarchical clustering of these data revealed that two of the non-crosslinked samples were outliers due to an unexpected high number of proteins identified (one sample for each genotype, Figures S1D and S1E, see also the section on Limitations of the Study). Consequently, we excluded these two samples from further analyses. Reanalysis of the remaining samples showed a clear separation of the crosslinked samples versus the non-crosslinked in the PCA (Figure 1C). Similar results were obtained by hierarchical clustering (Figure S1F). We measured a total of 2,473 proteins co-precipitating with RNA in WT worms and 2,219 proteins in the *vhl-1* mutant, respectively. 721 (WT) and 530 (*vhl-1* mutant) proteins were significantly enriched (student's ttest; FDR<0.05) in crosslinked over non-crosslinked samples (red dots in Figure 1D and blue dots in Figure 1E). Of note, we found an additional 371 (WT) and 305 (*vhl-1* mutant) proteins that were exclusively detected in crosslinked samples but never detected in non-crosslinked samples.

Identification of RNA-associated Proteins in WT and *vhl-1* Mutant Worms

In order to classify the proteins identified by levels of confidence we defined two different classes of RBPs. Proteins detected three times in the crosslinked samples in either genotype and never measured in the non-crosslinked samples are considered as class I RBPs. These proteins are not depicted in the volcano plots, as they do not have intensity values for the non-crosslinked samples (Figures 1D and 1E), but a list is provided in the online repository ("RBPome" tab, class I pulldown menu, http://shiny.cecad.uni-koeln.de:3838/celegans_rbpome) and in Table S1. Proteins with an FDR lower than 0.05 for enrichment in crosslinked samples (student's ttest) are defined as class II RBPs. Proteins not reaching the criteria for either class I or class II in our study that had been identified as RBPs in previous RIC experiments are defined as "other RBPs" (Hentze et al., 2018; Ignarski et al., 2019; Queiroz et al., 2019; Tamburino et al., 2013; Trendel et al., 2019; Urdaneta et al., 2019). All remaining proteins are summarized under the term "no evidence." We found that 45% of the proteins co-precipitated with RNA in WT and 38% of the proteins in the *vhl-1* mutant fall into either class I or class II (Figure 2A, "RBPome" tab http://shiny.cecad.uni-koeln.de:3838/celegans_rbpome and Table S1). In addition, we found that 788 proteins in WT and 963 proteins in *vhl-1* mutants were classified as "other RBPs," whereas the remaining 593 (WT) and 421 proteins (*vhl-1*) belong to the "no evidence" group (Figure 2A). For a general view on the nematode RBPome, the lists of proteins identified in either strain were pooled for enrichment analyses. For this purpose, the class II was assigned to RBPs classified differently between WT and *vhl-1* mutant (e.g. class I in *vhl-1* and class II in WT). Proteins

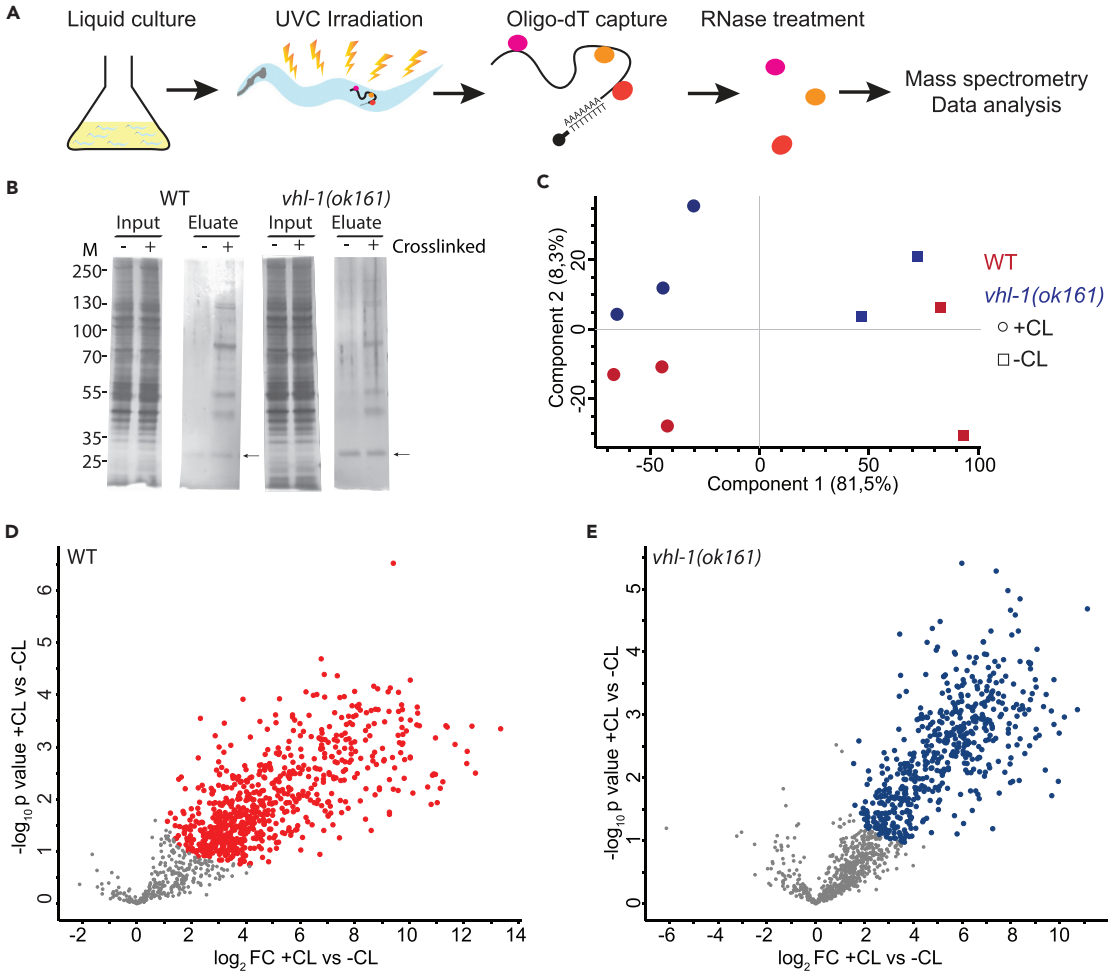

Figure 1. Identification of *C. elegans* RBPs Using RNA Interactome Capture

(A) Schematic overview of the RNA interactome capture protocol. Worms grown in liquid culture were UV-C (254 nm) irradiated; a non-irradiated sample was used as control. RNA-protein complexes were captured using oligo(dT) beads and analyzed by mass spectrometry after treatment with RNase I and Benzonase.

(B) Protein samples from WT and *vhl-1(ok161)* mutant worms were analyzed by SDS-PAGE and silver staining. Input and eluate of both crosslinked and non-crosslinked (−) samples (+) were directly compared. The band corresponding to RNase I and benzonase is indicated by an arrow. M: molecular weight marker (kDa).

(C) Principal component analysis (PCA) of the RIC mass spectrometry data (on the basis of iBAQ intensities). WT samples are indicated in red and *vhl-1(ok161)* mutants in blue. Crosslinked samples are indicated by circles and non-crosslinked samples by squares.

(D) Volcano plot depicting the t-test comparison of protein abundance in the crosslinked and non-crosslinked RIC dataset of WT worms. x-axis: $\log_2$ difference; y-axis: corresponding $-\log_{10}$ p-values. Seven hundred twenty-one significantly enriched proteins are shown in red (FDR<0.05). Proteins not reaching significance are shown in gray. FC: fold change; +CL: crosslinked; -CL: non-crosslinked; vs: versus.

(E) Corresponding volcano plot for the *vhl-1(ok161)* worm RIC dataset [for details see (D)]. Five hundred thirty significantly enriched proteins are shown in blue (FDR<0.05).

classified as class I or class II in one strain and assigned to "other RBPs" or "no evidence" in the other strain remained in their respective class (class I or class II) (Figure 2A, third bar). Gene ontology (GO) enrichment analyses of class I and class II revealed a striking overrepresentation of molecular function (MF) terms associated with RNA-binding underlining the validity of our dataset (Figure 2B). Additionally, other terms clearly linked to RNA metabolism were enriched in biological processes (BP) and cellular compartments (CC) (Figures S2A and S2B). In line with this finding, Pfam and SMART analyses of overrepresented protein domains showed RNA recognition motifs as the most enriched domain followed by other classical RNA-binding domains (Figures S2C and S2D).

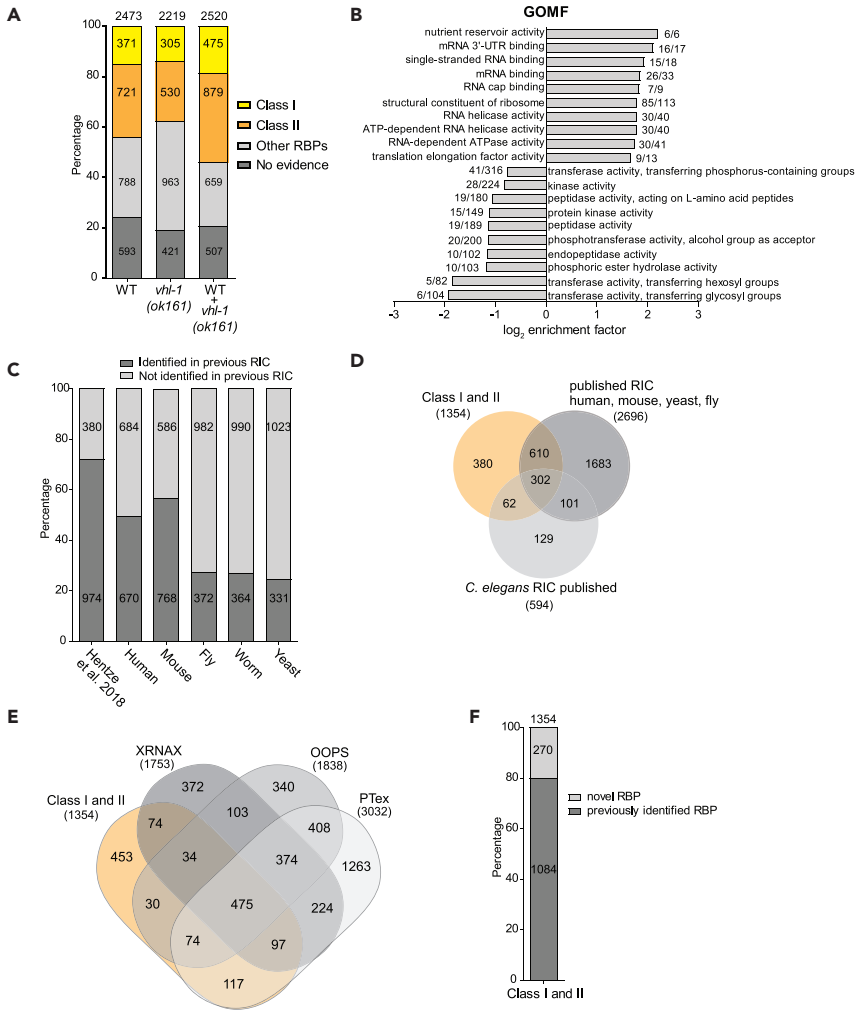

Figure 2. Comparison of the *C. elegans* RIC Dataset to Published RBPomes Reveals Novel RBPs

(A) Bar diagram showing the percentage of proteins contained in each class (class I: yellow, class II: orange, other RBPs: light gray, no evidence: dark gray). The total numbers of proteins measured are shown on top of each bar. The first two bars show data for each genotype only, whereas the third bar depicts combined data from both strains. Proteins measured by MS after RIC are classified depending on the level of confidence regarding their association with RNA.

(B) GO-term enrichment analysis (molecular function) of the combined RBPome from WT and *vhl-1* using the whole proteome as a background. Bar diagram depicting the top ten significant terms showing the highest and lowest enrichment factors (Fisher exact test; p-value<0.001). The numbers next to each bar indicate proteins contained in the RBPome followed by the size of the category.

(C) Comparison of the 1,354 RBPs (class I and II) identified in the pooled analysis from both *C. elegans* genotypes to published datasets. Dark gray: RBPs identified by previous RIC; light gray: previously not identified. Protein numbers are indicated in the respective bars.

(D) Comparison of the 1,354 RBPs (class I and II) identified in the pooled analysis from both *C. elegans* genotypes to the published worm RIC dataset (Matia-Gonzalez et al., 2015) and to a combined dataset of RBPs (previous RIC in human, mouse, yeast, fly [Hentze et al., 2018]). The total number of proteins contained in each dataset is indicated in brackets.

(E) Comparison of the 1,354 RBPs (class I and II) identified in the pooled analysis from both *C. elegans* genotypes to proteins identified by three novel techniques called protein-crosslinked RNA extraction (XRNAX), orthogonal organic phase separation (OOPS), and phenol toluol extraction (PTex) (Queiroz et al., 2019; Trendel et al., 2019). In brackets are reported the numbers of RBPs identified in the respective study.

(F) Bar diagram showing the percentage of known and novel RBPs in our dataset when pooling all comparisons to published studies (as specified in Figures 2C, 2E, and S2F).

Comparative Analyses with Published Datasets Reveal Novel RBPs in *C. elegans*

To further characterize the *C. elegans* RBPome, we performed an in-depth comparison to published datasets from different model organisms summarized in a recent study (Hentze et al., 2018) and complemented it with an RBPome of murine cells cultured under hypoxia (Ignarski et al., 2019). More than half of class I and class II proteins identified in our study had previously been identified by RIC screens (Figure 2C). In order to check whether our new dataset provided additional information to the only previously published *C. elegans* RBPome (Matia-Gonzalez et al., 2015), we compared both RBPomes with all RBPs identified in other species. This analysis revealed that our dataset confirmed 364 proteins as RBPs previously identified in the nematode and additionally 610 proteins previously identified as RBPs in other species (Figure 2D). Interestingly, most of the RBPs identified in our dataset were not predicted before in a study identifying putative nematode RBPs *in silico* (Figure S2E); this is in line with the fact that many RBPs do not contain classical RNA-binding domains (Beckmann et al., 2015; Tamburino et al., 2013). To complete this characterization, we compared our data with three recently published RBPome datasets using a novel methodology that—instead of RNA-pulldown targeting polyadenylated transcripts only—is based on purification of proteins crosslinked to the total RNA by organic extraction (Queiroz et al., 2019; Trendel et al., 2019; Urdaneta et al., 2019) (Figure 2E). Finally, taken together all these different comparisons, we can conclude that our dataset contains 1,084 previously described and 270 novel RBPs (Figure 2F, "RBPome" tab http://shiny.cecad.uni-koeln.de:3838/celegans_rbpome and Table S1).

Analysis of the Proteome of *vhl-1* Mutant Worms

To move our study toward a characterization of RBPs differentially regulated upon mutation of *vhl-1*, we performed MS on whole worm lysates obtained from WT and *vhl-1* mutants (RICs input). PCA and hierarchical clustering of these data showed a clear separation by genotype (Figures 3A and S3A). In total, we identified 5,759 proteins, 153 of which were differentially expressed between *vhl-1* mutant and WT worms (student's ttest; FDR<0.05) (Figure 3B, "Proteome *vhl-1* vs WT" tab http://shiny.cecad.uni-koeln.de:3838/celegans_rbpome and Table S1). Importantly, both HIF-1 itself as well as known HIF-1 target genes are more abundant in *vhl-1* mutants (Figure 3B, black dots) (Dengler et al., 2014; Ortiz-Barahona et al., 2010; Semenza, 2012; Shen et al., 2005). A GO term enrichment analysis of the significantly regulated proteins revealed that biological processes known to be modulated by HIF-1 such as defense, immune response, and CoA desaturase activity were overrepresented (Figures 3C, S3B, and S3C) (Krzywinska and Stockmann, 2018; Palazon et al., 2014; Zhang et al., 2013). Comparing the differentially expressed proteins with our RBPome dataset, we found only 12 RBPs that differ in abundance on the protein level (student's ttest; FDR<0.05) (Figure 3D).

Modulation of the RBPome by *vhl-1* Loss-of-Function

The classification of proteins identified by RIC in the two different strains as shown in the bar diagram in Figure 2A depends on arbitrary thresholds. Consequently, proteins detected only in one of the strains based on these thresholds are not necessarily specific to this condition. To allow for a more exhaustive view on hypoxia-signaling-associated RNA-protein binding events, we performed an in-depth analysis of this aspect using the following strategy. Analyzing the data from crosslinked samples in RIC, we found five proteins that were measured in all three *vhl-1* crosslinked samples but never measured in WT (both + and − crosslinking) (Figure 4A). Importantly, the abundance of these proteins in the proteome is not affected by mutation of *vhl-1*, suggesting that the different efficiency in the pulldown observed indeed depends on differential binding of RNA molecules (Figure S4A). Additionally, we found 24 RBPs that were measured exclusively in all WT crosslinked samples but never in *vhl-1* (Figure 4B). Again, the abundance of these 24 proteins was not affected by genotype on the protein level (Figure S4B). To extend the comparison to proteins detected in both genotypes we calculated for WT (crosslinked vs non-crosslinked) versus *vhl-1* (crosslinked vs non-crosslinked), the linear regression, and the 95% prediction interval from $\log_2$ fold changes (for detailed information see Transparent Methods). Proteins outside the 95% prediction interval were considered to be more strongly enriched in either WT or *vhl-1* mutant worms (Figure 4C and Table S1) ("Proteome WT vs. *vhl-1*" tab http://shiny.cecad.uni-koeln.de:3838/celegans_rbpome). Performing this analysis, 25 RBPs were more enriched in *vhl-1* mutants (blue) and 26 RBPs in WT (red) worms. The abundance of the 25 RBPs enriched in *vhl-1* mutants was not affected by genotype on the protein level and only 1 (H28G03.1) out of the 26 proteins enriched in WT showed a difference in protein abundance (Figures S4C and S4D). Interestingly, this protein—H28G03.1, an orthologue of human HNRNPA proteins—was enriched in the pulldown from crosslinked WT samples but showed higher protein abundance in *vhl-1* mutant worms pointing toward opposite modes of regulation regarding protein levels and RNA-binding capacity.

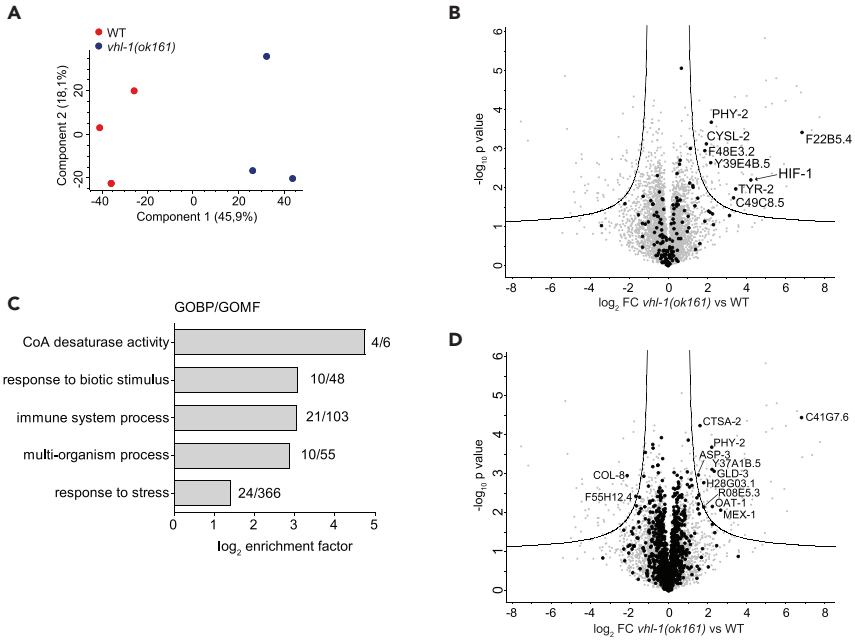

Figure 3. RBPs Differentially Regulated in *vhl-1* Mutant Worms Proteome

(A) PCA of the proteome mass spectrometry data (on the basis of iBAQ intensities). WT samples are indicated in red and *vhl-1*(*ok161*) mutants in blue.

(B) Volcano plot illustrating the differentially expressed proteins between the proteomes of *vhl-1*(*ok161*) mutant and WT worms. The -$\log_{10}$ p-value is plotted on the y-axis. The $\log_2$ fold change (*vhl-1*(*ok161*) vs WT) is indicated on the x-axis. Proteins above the cutoff line are considered significant (student's ttest; FDR<0.05). Black dots: known HIF-1 targets (Dengler et al., 2014; Ortiz-Barahona et al., 2010; Shen et al., 2005), differentially expressed HIF-1 targets are indicated by name; HIF-1 itself is indicated by the arrow; gray dots: other proteins. Total number of proteins = 5759.

(C) Bar diagram shows the top five GO-terms with the highest enrichment factor (Fisher exact test; p-value<0.001). Biological processes (GOBP) and molecular function (GOMF) of the significantly regulated proteins in the proteome are depicted. The numbers indicate the proteins in the category followed by category size.

(D) Volcano plot illustrating the differentially expressed proteins between the proteomes of *vhl-1*(*ok161*) mutant worms and WT worms. The -$\log_{10}$ p-value is plotted on the y-axis and the $\log_2$ fold change (*vhl-1*(*ok161*) vs WT) on the x-axis. Proteins above the cutoff line are considered significant (student's ttest; FDR<0.05). Class I and II RBPs from WT and *vhl-1*(*ok161*) mutant worms are shown in black, differentially expressed RBPs are indicated by name.

DISCUSSION

Recently, the global landscape of RBPs has been addressed in many organisms from yeast to mammals using RIC (Hentze et al., 2018). Whereas studies on mammalian RBPs—due to availability and feasibility—focused on cultured cells (Baltz et al., 2012; Beckmann et al., 2015; Castello et al., 2012; Kwon et al., 2013; Liepelt et al., 2016; Schueler et al., 2014), the RBPome of multicellular organisms has been described for the fruit fly, nematode, *Arabidopsis thaliana*, and zebrafish so far (Despic et al., 2017; Marondedze et al., 2016; Matia-Gonzalez et al., 2015; Reichel et al., 2016; Sysoev et al., 2016; Wessels et al., 2016). Data regarding the *C. elegans* RBPome is available from a study published by Matia-Gonzalez et al. that used UV-C crosslinking and RIC in mixed-stage worms as well as L4 larvae after induction of apoptosis (Matia-Gonzalez et al., 2015). In our study, we describe the first *C. elegans* RBPome from young adult worms using two different genotypes. Employing stringent filtering criteria this approach identified 1354 RBPs, around 26% of which had been described by Matia-Gonzalez before. This finding underlines the importance of performing RIC in different biological and technical conditions to obtain a global view on the RBPome of a specific organism. However, the majority of our RBPs is not entirely novel and had been identified in cells from other species before showing the validity of our dataset. Two hundred seventy proteins had not been described in any other published RIC study leading to their classification as novel RBPs. Their novelty may be attributed to a couple of different reasons. First, only about half of them are conserved in mammals, making their identification impossible in most of the previous screens. Second, technical differences, especially regarding MS and data analysis, may account for this finding. Third, and very importantly in our view,

A

WB Gene ID	Gene Name	Human Ortholog	RBPome Class	novel RBP	Function
WBGene00006442	*tag-65*	*CHERP*	I		calcium homeostasis endoplasmic reticulum protein
WBGene00009498	*tat-5*	*ATP9B;ATP9A*	I	+	ATPase phospholipid transporting
WBGene00010730	*ensa-1*	*ARPP19;ENSA*	I		protein phosphatase inhibitor
WBGene00015203	*B0495.2*	*CDK11A*	I		cyclin dependent kinase
WBGene00022488	*orc-3*	n.a.	I	+	n.a.

B

WB Gene ID	Gene Name	Human Ortholog	RBPome Class	novel RBP	Function
WBGene00002994	*lin-5*	n.a.	I	+	dynein complex binding
WBGene00008119	*C46F11.4*	*DDX42*	I		ATP binding
WBGene00008412	*D2030.2*	*CLPX*	I		ATP binding
WBGene00008694	*vwa-8*	*VWA8*	I	+	ATP binding
WBGene00009221	*acs-2*	*ACSF2*	I		acyl-CoA synthetase
WBGene00009259	*hpo-34*	n.a.	I	+	n.a.
WBGene00009290	*F31D4.2*	*ARMT1*	I	+	S-adenosylmethionine-depent methytransferase
WBGene00009740	*F45H10.3*	*NDUFA7*	I		NADH dehydrogenase
WBGene00010015	*atad-3*	*ATAD3A*	I		ATP binding
WBGene00010766	*mrps-27*	*MRPS27*	I		mitochondrial ribosome binding
WBGene00011743	*T13F2.2*	*SUB1*	I		DNA binding
WBGene00012156	*ebp-2*	*MAPRE1*	I		microtubule binding
WBGene00012996	*pinn-4*	*PIN4*	I		peptidyl-prolyl cis-trans isomerase
WBGene00013040	*Y49E10.21*	n.a.	I	+	n.a.
WBGene00013477	*Y69E1A.5*	*PEBP1*	I		protein kinase binding
WBGene00014108	*ZK856.7*	n.a.	I	+	n.a.
WBGene00016419	*tyr-4*	*TYR*	I	+	metal ion binding
WBGene00018682	*aagr-4*	*GANAB;GANC*	I		carbohydrate binding and hydrolyzing O-glycosyl
WBGene00019005	*F57B10.8*	*ABT1*	I		RNA binding
WBGene00019478	*tag-225*	*TIMP2;TIMP3;TIMP1;TIMP4*	I		metalloendopeptidase inhibitor
WBGene00020104	*R148.5*	n.a.	I	+	n.a.
WBGene00020112	*pfd-5*	*PFDN5*	I		unfolded protein binding
WBGene00006583	*tnc-2*	*TNNC2*	II	+	troponin I binding
WBGene00016415	*ampd-1*	*AMPD2*	II		AMP deminase

C

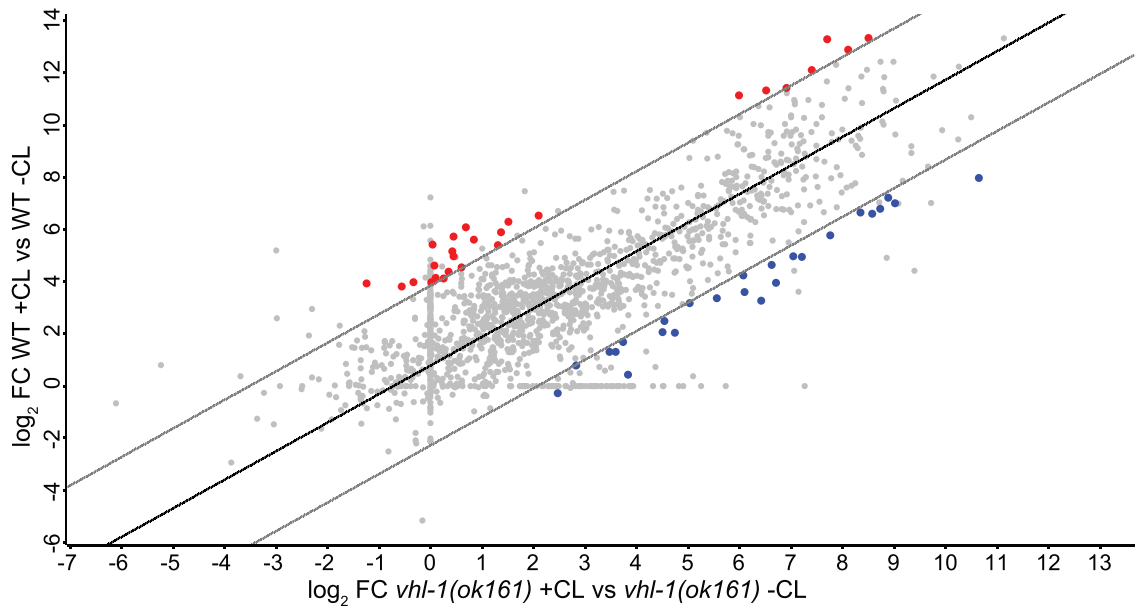

Figure 4. Loss of VHL-1 Leads to Quantitative and Qualitative Changes in the RBPome

(A) Table of RBPs detected exclusively in all three *vhl-1(ok161)* crosslinked samples but never detected in WT. Depicted are: wormbase (WB) gene ID, gene name, human ortholog name, RBPome class (indicated by I [class I] or II [class II]), novel RBP (indicated by +), and the function; n.a., not available.

(B) Table depicting RBPs detected exclusively in all three WT crosslinked samples but never detected in *vhl-1(ok161)* (for table details see A.).

Figure 4. *Continued*

(C) Scatterplot showing the correlation of log_2 fold changes of *vhl-1(ok161)* RBPs (crosslinked vs non-crosslinked) on the x-axis and WT (crosslinked vs non-crosslinked) samples on the y-axis. FC, fold change; +CL, crosslinked; -CL, non-crosslinked; vs, versus. The linear regression was calculated with R (black line, deming() method, formula: y = 0.7806137 + 1.095646*x). Proteins outside the calculated 95% prediction interval (gray lines) are considered to be more strongly enriched after RIC in one of the two strains, suggesting a regulation of the binding to target RNAs in WT or *vhl-1(ok161)*. Blue dots: proteins more enriched in *vhl-1*(*ok161*); red dots: proteins more enriched in WT; gray dots: not in class I or class II.

both expression and RNA-binding capacity of specific RBPs can be context specific, leading to their first description in synchronized young adult and *vhl-1* knockout worms. In this context, dynamic modulation of the RBPome is a highly interesting research question. The use of *vhl-1* mutants allowed us to obtain a first view on changes in the RBP landscape upon genetic activation of HIF-signaling. There are several lines of evidence linking HIF-signaling to RNA-protein binding events. On the one hand, RBPs can have an impact on HIF expression itself. The human antigen R (HuR) binds to the 5′untranslated region (UTR) of HIF-1α mRNA and thereby promotes it translation (Galban et al., 2008). Another study showed that the RBP RBM38 is able to bind HIF1α mRNA via binding to HIF1α 5′ and -3′′UTRs. Moreover, knockdown of RBM38 increased the level of HIF-1α protein under hypoxic conditions (Cho et al., 2015). On the other hand, it is known that hypoxia can lead to repression of cap-mediated translation, involving RBPs (Uniacke et al., 2012). This phenomenon can be overruled for transcripts that are important to the response to hypoxia through an HIF-2α-RBM4-eIF4E2 complex that binds to these mRNAs and targets them to polysomes for translation (Uniacke et al., 2012). Furthermore, recently published work from our group showed modulation of the RBPome by hypoxia in cultured cells (Ignarski et al., 2019). Consequently, hypoxia signaling appeared as an attractive target to be studied in a genetic model of *C. elegans*. Here, it should be noted that we observed a reduced RNA and protein yield in *vhl-1* mutant worms. Mutation of *vhl-1* has been shown before to lead to a smaller size of the nematode (Wen et al., 2015), which may be the underlying reason for the unexpected lower yield. However, due to the similar amount of RNA after pulldown in both strains and conditions we do not expect this to have an impact on the results of our RIC. Analysis of the proteome confirmed HIF-1 to be stabilized and significantly upregulated in *vhl-1* mutant worms. It is important to note that our study cannot dissect RBPs affected by activation of HIF-signaling from those that may be affected by loss of *vhl-1* directly. Considering that most changes in these mutants are generally assumed to be mediated by HIF-1, it is likely that this is the case for the majority of changes we observed as well. However, final proof of this will require future experiments using either *vhl-1; hif-1* double mutant worms or different means of HIF activation, e.g. expression of a stabilized version of HIF-1. To allow for a first insight into evolutionary conservation of hypoxia-signaling-associated modulation of RBPs we compared the results in this study with our previous findings in cultured cells under hypoxia (Ignarski et al., 2019). Based on the results in Figure 4 of the study at hand, we did not find any obvious overlap regarding the modulation of RNA-binding. This is well explained by several key differences in experimental design. In Ignarski et al., HIF activation was performed by short-term exposure of cultured mIMCD3 cells to hypoxia, whereas HIF-signaling is permanently activated in *vhl-1* mutants. However, when comparing all RBPs that show a hypoxia-modulated RNA-binding capacity in cultured cells with the *C. elegans* RBPomes, we found two RBPs showing similar changes in both studies. On the one hand, CCT-1—a component of the TCP1 chaperonin complex—reaches statistical significance as class II RBP only in WT but not in the *vhl-1* mutant (see ''RBPome'' tab http://shiny.cecad.uni-koeln.de:3838/celegans_rbpome and Table S1). In line with this finding, the mouse ortholog, TCP1, is identified as an RBP only in normoxic cultured cells (Ignarski et al., 2019). TCP1 is well known to be dedicated to the folding of actin and tubulin (Sternlicht et al., 1993; Vallin and Grantham, 2019). Interestingly, TCP1 mediates also the folding and assembly of VHL into a complex with its partner proteins (Feldman et al., 1999), showing its importance in HIF-singling. On the other hand, PRO-3 only reaches significance as an RBP in *vhl-1* mutant worms (see ''RBPome'' tab http://shiny.cecad.uni-koeln.de:3838/celegans_rbpome and Table S1). Its mouse orthologue—SDAD1, a protein required for 60S pre-ribosomal subunit export to the cytoplasm—did only reach the criteria of an RBP in cells after hypoxia (Ignarski et al., 2019). SDAD1 is implicated in regulation of tumor progression and metastasis (Ding et al., 2018; Zeng et al., 2017). There is an indication that HuR, an RBP targeting HIF-1 mRNA (Galban et al., 2008), also binds to SDAD1 mRNA (Jing et al., 2019). It will now be of great interest to focus on the function of specific hypoxia-modulated RBPs such as SDAD1 and TCP1 and to further characterize their differential RNA-binding, e.g. using crosslinking and immunoprecipitation protocols. This will not only allow for distinguishing differential RNA-binding capacity from differential availability of the actual mRNA targets as being the reason for the observed hypoxia-associated changes but also be the first step toward elucidating the biological consequences of hypoxia-induced alterations of these RNA-protein binding events.

Limitations of the Study

In the present study, we found significantly lower RNA and protein yields in *vhl-1* mutants using equal numbers of worms. The reasons for this finding are not examined here but can be hypothesized based on published data. Firstly, Wen et al. described that *vhl-1* mutants are shorter compared with WT (Wen et al., 2015). Secondly, it is well known that loss of *vhl-1* induces longevity (Mehta et al., 2009; Muller et al., 2009; Zhang et al., 2009). Ewald et al. reported a direct link between collagen abundance and longevity (Ewald et al., 2015). Furthermore, the mammalian orthologue of VHL-1 is known to have an impact on extracellular matrix formation (Kurban et al., 2008). Changes in the worm cuticle could lead to differences in the efficiency of RNA and protein extraction. Although this issue does not affect the RNA yield after pulldown, we cannot exclude a resulting bias introduced into the comparison between WT worms and *vhl-1* mutants. More experiments will be required to address this aspect conclusively. Our analysis of RBPs in *C. elegans* started with three biological replicates of crosslinked and non-crosslinked WT and *vhl-1* mutant samples. However, one non-crosslinked sample of each genotype showed a much higher number of proteins identified by MS than expected (even more than in the corresponding crosslinked samples), potentially due to contamination with whole worm lysate. These samples were excluded from the analysis. The RBPome analysis is therefore based on three biological replicates of crosslinked and two non-crosslinked WT and *vhl-1* mutant samples. Notably, previously published RIC studies also gained reliable data using two replicates and even pooled non-crosslinked data from different conditions due to high similarity (Baltz et al., 2012; Castello et al., 2012; Liepelt et al., 2016; Mitchell et al., 2013).

METHODS

All methods can be found in the accompanying Transparent Methods supplemental file.

DATA AND CODE AVAILABILITY

The mass spectrometry data (Raw data and MaxQuant [version 1.5.3.8] output) have been deposited to the ProteomeXchange Consortium (http://www.ebi.ac.uk/pride) via the PRIDE (Perez-Riverol et al., 2019) partner repository with the dataset identifier PXD014469.

An interactive online repository was created and is provided at http://shiny.cecad.uni-koeln.de:3838/celegans_rbpome.

SUPPLEMENTAL INFORMATION

Supplemental Information can be found online at https://doi.org/10.1016/j.isci.2019.11.039.

ACKNOWLEDGMENTS

We thank Serena Greco-Torres for excellent technical assistance. The *C. elegans* strains were provided by the CGC, which is funded by NIH Office of Research Infrastructure Programs (P40 OD010440). This work was supported by the Nachwuchsgruppen NRW program of the Ministry of Science North Rhine Westfalia (MIWF, to R.-U.M.) and the German Research Foundation (DFG; MU3629/2–1). R.-U.M., T.B. and B.S. received additional funding from the German Research Foundation (DFG; MU3629/3-1 to R.-U.M., BE2212 and KFO329 to T.B., SCHE1562/6 to B.S.).

AUTHOR CONTRIBUTIONS

F.F. and R.-U.M. designed the study; R.E., T.K., D.A, and L.S. performed experiments; R.E. K.B., and F.F. analyzed the data; R.E., M.I., K.B., R.-U.M., and F.F. prepared the figures; R.E., M.I., R.-U.M., T.B., B.S., and F.F. drafted and revised the paper; all authors approved the final version of the manuscript.

DECLARATION OF INTERESTS

The authors declare no competing interests.

Received: August 9, 2019
Revised: September 17, 2019
Accepted: November 21, 2019
Published: December 20, 2019

REFERENCES

Baltz, A.G., Munschauer, M., Schwanhausser, B., Vasile, A., Murakawa, Y., Schueler, M., Youngs, N., Penfold-Brown, D., Drew, K., Milek, M., et al. (2012). The mRNA-bound proteome and its global occupancy profile on protein-coding transcripts. Mol.Cell *46*, 674–690.

Beckmann, B.M., Horos, R., Fischer, B., Castello, A., Eichelbaum, K., Alleaume, A.M., Schwarzl, T., Curk, T., Foehr, S., Huber, W., et al. (2015). The RNA-binding proteomes from yeast to man harbour conserved enigmRBPs. Nat. Commun. *6*, 10127.

Castello, A., Fischer, B., Eichelbaum, K., Horos, R., Beckmann, B.M., Strein, C., Davey, N.E., Humphreys, D.T., Preiss, T., Steinmetz, L.M., et al. (2012). Insights into RNA biology from an atlas of mammalian mRNA-binding proteins. Cell *149*, 1393–1406.

Cho, S.J., Teng, I.F., Zhang, M., Yin, T., Jung, Y.S., Zhang, J., and Chen, X. (2015). Hypoxia-inducible factor 1 alpha is regulated by RBM38, a RNA-binding protein and a p53 family target, via mRNA translation. Oncotarget *6*, 305–316.

Dengler, V.L., Galbraith, M., and Espinosa, J.M. (2014). Transcriptional regulation by hypoxia inducible factors. Crit. Rev. Biochem. Mol. Biol. *49*, 1–15.

Despic, V., Dejung, M., Gu, M., Krishnan, J., Zhang, J., Herzel, L., Straube, K., Gerstein, M.B., Butter, F., and Neugebauer, K.M. (2017). Dynamic RNA-protein interactions underlie the zebrafish maternal-to-zygotic transition. Genome Res. *27*, 1184–1194.

Ding, Z., Lan, H., Xu, R., Zhou, X., and Pan, Y. (2018). LncRNA TP73-AS1 accelerates tumor progression in gastric cancer through regulating miR-194-5p/SDAD1 axis. Pathol. Res. Pract. *214*, 1993–1999.

Ewald, C.Y., Landis, J.N., Porter Abate, J., Murphy, C.T., and Blackwell, T.K. (2015). Dauer-independent insulin/IGF-1-signalling implicates collagen remodelling in longevity. Nature *519*, 97–101.

Feldman, D.E., Thulasiraman, V., Ferreyra, R.G., and Frydman, J. (1999). Formation of the VHL-elongin BC tumor suppressor complex is mediated by the chaperonin TRiC. Mol.Cell *4*, 1051–1061.

Fredericks, A.M., Cygan, K.J., Brown, B.A., and Fairbrother, W.G. (2015). RNA-binding proteins: splicing factors and disease. Biomolecules *5*, 893–909.

Galban, S., Kuwano, Y., Pullmann, R., Jr., Martindale, J.L., Kim, H.H., Lal, A., Abdelmohsen, K., Yang, X., Dang, Y., Liu, J.O., et al. (2008). RNA-binding proteins HuR and PTB promote the translation of hypoxia-inducible factor 1alpha. Mol.Cell Biol. *28*, 93–107.

Halbeisen, R.E., Galgano, A., Scherrer, T., and Gerber, A.P. (2008). Post-transcriptional gene regulation: from genome-wide studies to principles. Cell Mol. Life Sci. *65*, 798–813.

Hall, T.M. (2005). Multiple modes of RNA recognition by zinc finger proteins. Curr. Opin. Struct. Biol. *15*, 367–373.

Hasan, A., Cotobal, C., Duncan, C.D., and Mata, J. (2014). Systematic analysis of the role of RNA-binding proteins in the regulation of RNA stability. PLoS Genet. *10*, e1004684.

Hentze, M.W., Castello, A., Schwarzl, T., and Preiss, T. (2018). A brave new world of RNA-binding proteins. Nat. Rev. Mol.Cell Biol. *19*, 327–341.

Ignarski, M., Rill, C., Kaiser, R.W.J., Kaldirim, M., Neuhaus, R., Esmaillie, R., Li, X., Klein, C., Bohl, K., Petersen, M., et al. (2019). The RNA-protein interactome of differentiated kidney tubular epithelial cells. J. Am. Soc. Nephrol. *30*, 564–576.

Jiang, H., Xu, L., Wang, Z., Keene, J., and Gu, Z. (2014). Coordinating expression of RNA binding proteins with their mRNA targets. Sci. Rep. *4*, 7175.

Jing, L., Li, S., Wang, J., and Zhang, G. (2019). Long non-coding RNA small nucleolar RNA host gene 7 facilitates cardiac hypertrophy via stabilization of SDA1 domain containing 1 mRNA. J.Cell Biochem. *120*, 15089–15097.

Kaelin, W.G. (2005). Proline hydroxylation and gene expression. Annu. Rev. Biochem. *74*, 115–128.

Kechavarzi, B., and Janga, S.C. (2014). Dissecting the expression landscape of RNA-binding proteins in human cancers. Genome Biol. *15*, R14.

Krzywinska, E., and Stockmann, C. (2018). Hypoxia, metabolism and immune cell function. Biomedicines *6*, 2–3.

Kurban, G., Duplan, E., Ramlal, N., Hudon, V., Sado, Y., Ninomiya, Y., and Pause, A. (2008). Collagen matrix assembly is driven by the interaction of von Hippel-Lindau tumor suppressor protein with hydroxylated collagen IV alpha 2. Oncogene *27*, 1004–1012.

Kwon, S.C., Yi, H., Eichelbaum, K., Fohr, S., Fischer, B., You, K.T., Castello, A., Krijgsveld, J., Hentze, M.W., and Kim, V.N. (2013). The RNA-binding protein repertoire of embryonic stem cells. Nat. Struct. Mol. Biol. *20*, 1122–1130.

Lee, S.R., and Lykke-Andersen, J. (2013). Emerging roles for ribonucleoprotein modification and remodeling in controlling RNA fate. Trends Cell Biol *23*, 504–510.

Liepelt, A., Naarmann-de Vries, I.S., Simons, N., Eichelbaum, K., Fohr, S., Archer, S.K., Castello, A., Usadel, B., Krijgsveld, J., Preiss, T., et al. (2016). Identification of RNA-binding proteins in macrophages by interactome capture. Mol.Cell Proteomics *15*, 2699–2714.

Lukong, K.E., Chang, K.W., Khandjian, E.W., and Richard, S. (2008). RNA-binding proteins in human genetic disease. Trends Genet. *24*, 416–425.

Luo, D., Wang, Z., Wu, J., and Jiang, C. (2014). The role of hypoxia inducible factor-1 in hepatocellular carcinoma. Biomed. Res. Int. *2014*, 409272.

Marondedze, C., Thomas, L., Serrano, N.L., Lilley, K.S., and Gehring, C. (2016). The RNA-binding protein repertoire of Arabidopsis thaliana. Sci. Rep. *6*, 29766.

Matia-Gonzalez, A.M., Laing, E.E., and Gerber, A.P. (2015). Conserved mRNA-binding proteomes in eukaryotic organisms. Nat. Struct. Mol. Biol. *22*, 1027–1033.

Maxwell, P.H., Wiesener, M.S., Chang, G.W., Clifford, S.C., Vaux, E.C., Cockman, M.E., Wykoff, C.C., Pugh, C.W., Maher, E.R., and Ratcliffe, P.J. (1999). The tumour suppressor protein VHL targets hypoxia-inducible factors for oxygen-dependent proteolysis. Nature *399*, 271–275.

Mehta, R., Steinkraus, K.A., Sutphin, G.L., Ramos, F.J., Shamieh, L.S., Huh, A., Davis, C., Chandler-Brown, D., and Kaeberlein, M. (2009). Proteasomal regulation of the hypoxic response modulates aging in C. elegans. Science *324*, 1196–1198.

Mitchell, S.F., Jain, S., She, M., and Parker, R. (2013). Global analysis of yeast mRNPs. Nat. Struct. Mol. Biol. *20*, 127–133.

Muller, R.U., Fabretti, F., Zank, S., Burst, V., Benzing, T., and Schermer, B. (2009). The von Hippel Lindau tumor suppressor limits longevity. J. Am. Soc. Nephrol. *20*, 2513–2517.

Ortiz-Barahona, A., Villar, D., Pescador, N., Amigo, J., and del Peso, L. (2010). Genome-wide identification of hypoxia-inducible factor binding sites and target genes by a probabilistic model integrating transcription-profiling data and in silico binding site prediction. Nucleic Acids Res. *38*, 2332–2345.

Palazon, A., Goldrath, A., Nizet, V., and Johnson, R.S. (2014). HIF transcription factors, inflammation, and immunity. Immunity *41*, 518–528.

Perez-Riverol, Y., Csordas, A., Bai, J., Bernal-Llinares, M., Hewapathirana, S., Kundu, D.J., Inuganti, A., Griss, J., Mayer, G., Eisenacher, M., et al. (2019). The PRIDE database and related tools and resources in 2019: improving support for quantification data. Nucleic Acids Res. *47*, D442–d450.

Queiroz, R.M.L., Smith, T., Villanueva, E., Marti-Solano, M., Monti, M., Pizzinga, M., Mirea, D.M., Ramakrishna, M., Harvey, R.F., Dezi, V., et al. (2019). Comprehensive identification of RNA-protein interactions in any organism using orthogonal organic phase separation (OOPS). Nat. Biotechnol. *37*, 169–178.

Query, C.C., Bentley, R.C., and Keene, J.D. (1989). A common RNA recognition motif identified within a defined U1 RNA binding domain of the 70K U1 snRNP protein. Cell *57*, 89–101.

Reichel, M., Liao, Y., Rettel, M., Ragan, C., Evers, M., Alleaume, A.M., Horos, R., Hentze, M.W., Preiss, T., and Millar, A.A. (2016). In planta determination of the mRNA-binding proteome of Arabidopsis etiolated seedlings. Plant Cell *28*, 2435–2452.

Schueler, M., Munschauer, M., Gregersen, L.H., Finzel, A., Loewer, A., Chen, W., Landthaler, M., and Dieterich, C. (2014). Differential protein occupancy profiling of the mRNA transcriptome. Genome Biol. *15*, R15.

Semenza, G.L. (2012). Hypoxia-inducible factors: mediators of cancer progression and targets for cancer therapy. Trends Pharmacol. Sci. *33*, 207–214.

Shen, C., Nettleton, D., Jiang, M., Kim, S.K., and Powell-Coffman, J.A. (2005). Roles of the HIF-1 hypoxia-inducible factor during hypoxia response in Caenorhabditis elegans. J. Biol. Chem. *280*, 20580–20588.

Sternlicht, H., Farr, G.W., Sternlicht, M.L., Driscoll, J.K., Willison, K., and Yaffe, M.B. (1993). The t-complex polypeptide 1 complex is a chaperonin for tubulin and actin in vivo. Proc. Natl. Acad. Sci. U S A *90*, 9422–9426.

Sysoev, V.O., Fischer, B., Frese, C.K., Gupta, I., Krijgsveld, J., Hentze, M.W., Castello, A., and Ephrussi, A. (2016). Global changes of the RNA-bound proteome during the maternal-to-zygotic transition in Drosophila. Nat. Commun. *7*, 12128.

Tamburino, A.M., Ryder, S.P., and Walhout, A.J. (2013). A compendium of Caenorhabditis elegans RNA binding proteins predicts extensive regulation at multiple levels. G3 (Bethesda) *3*, 297–304.

Trendel, J., Schwarzl, T., Horos, R., Prakash, A., Bateman, A., Hentze, M.W., and Krijgsveld, J. (2019). The human RNA-binding proteome and its dynamics during translational arrest. Cell *176*, 391–403.e19.

Uniacke, J., Holterman, C.E., Lachance, G., Franovic, A., Jacob, M.D., Fabian, M.R., Payette, J., Holcik, M., Pause, A., and Lee, S. (2012). An oxygen-regulated switch in the protein synthesis machinery. Nature *486*, 126–129.

Urdaneta, E.C., Vieira-Vieira, C.H., Hick, T., Wessels, H.H., Figini, D., Moschall, R., Medenbach, J., Ohler, U., Granneman, S., Selbach, M., et al. (2019). Purification of cross-linked RNA-protein complexes by phenol-toluol extraction. Nat. Commun. *10*, 990.

Vallin, J., and Grantham, J. (2019). The role of the molecular chaperone CCT in protein folding and mediation of cytoskeleton-associated processes: implications for cancer cell biology. Cell Stress Chaperones *24*, 17–27.

Wen, H., Yu, Y., Zhu, G., Jiang, L., and Qin, J. (2015). A droplet microchip with substance exchange capability for the developmental study of C. elegans. Lab. Chip *15*, 1905–1911.

Wessels, H.H., Imami, K., Baltz, A.G., Kolinski, M., Beldovskaya, A., Selbach, M., Small, S., Ohler, U., and Landthaler, M. (2016). The mRNA-bound proteome of the early fly embryo. Genome Res. *26*, 1000–1009.

Wilkie, G.S., Dickson, K.S., and Gray, N.K. (2003). Regulation of mRNA translation by 5'- and 3'-UTR-binding factors. Trends Biochem. Sci. *28*, 182–188.

Zeng, M., Zhu, L., Li, L., and Kang, C. (2017). miR-378 suppresses the proliferation, migration and invasion of colon cancer cells by inhibiting SDAD1. Cell Mol. Biol. Lett. *22*, 12.

Zhang, B., Gallegos, M., Puoti, A., Durkin, E., Fields, S., Kimble, J., and Wickens, M.P. (1997). A conserved RNA-binding protein that regulates sexual fates in the C. elegans hermaphrodite germ line. Nature *390*, 477–484.

Zhang, Y., Shao, Z., Zhai, Z., Shen, C., and Powell-Coffman, J.A. (2009). The HIF-1 hypoxia-inducible factor modulates lifespan in C. elegans. PLoS One *4*, e6348.

Zhang, Y., Wang, H., Zhang, J., Lv, J., and Huang, Y. (2013). Positive feedback loop and synergistic effects between hypoxia-inducible factor-2alpha and stearoyl-CoA desaturase-1 promote tumorigenesis in clear cell renal cell carcinoma. Cancer Sci. *104*, 416–422.

ISCI, Volume *22*

Supplemental Information

Activation of Hypoxia-Inducible Factor Signaling Modulates the RNA Protein Interactome in *Caenorhabditis elegans*

Reza Esmaillie, Michael Ignarski, Katrin Bohl, Tim Krüger, Daniyal Ahmad, Lisa Seufert, Bernhard Schermer, Thomas Benzing, Roman-Ulrich Müller, and Francesca Fabretti

Figure S1

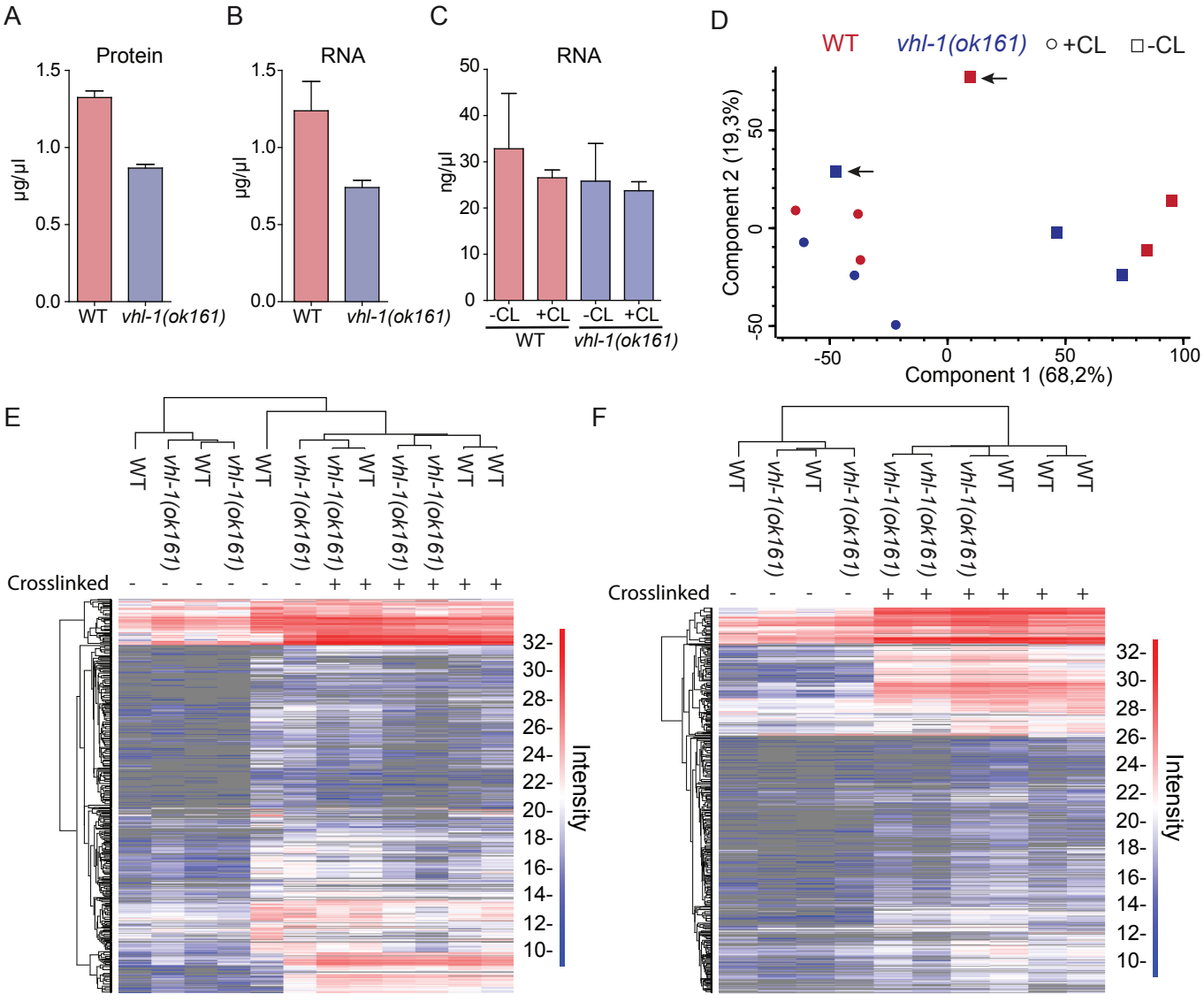
A
Protein
µg/µl
1.5
1.0
0.5
0.0
WT
vhl-1(ok161)
B
RNA
µg/µl
1.5
1.0
0.5
0.0
WT
vhl-1(ok161)
C
RNA
ng/µl
50
40
30
20
10
0
-CL
+CL
-CL
+CL
WT
vhl-1(ok161)
D
WT
vhl-1(ok161)
+CL
-CL
Component 2 (19,3%)
50
0
-50
-50
0
50
100
Component 1 (68,2%)
E
WT
vhl-1(ok161)
WT
vhl-1(ok161)
WT
vhl-1(ok161)
vhl-1(ok161)
WT
vhl-1(ok161)
WT
WT
Crosslinked
- - - - - - + + + + + +
32-
30-
28-
26-
24-
22-
20-
18-
16-
14-
12-
10-
Intensity
F
WT
vhl-1(ok161)
WT
vhl-1(ok161)
vhl-1(ok161)
vhl-1(ok161)
vhl-1(ok161)
WT
WT
WT
Crosslinked
- - - - + + + + + +
32-
30-
28-
26-
24-
22-
20-
18-
16-
14-
12-
10-
Intensity

Figure S1. Analysis of RNA Interactome capture samples, Related to Figure 1

A. Quantification of the protein yield from 500 WT or *vhl-1(ok161)* mutant worms. Data are represented as mean ± SEM of three biological replicates. **B.** Quantification of the corresponding RNA yield from 500 WT or *vhl-1(ok161)* mutant worms. Data are represented as mean ± SEM of three biological replicates. **C.** Quantification of RNA in RIC eluates from WT and *vhl-1(ok161)* mutant worms before RNase digestion. Crosslinked samples (+CL) were compared to non-crosslinked samples (-CL). Data are represented as mean ± SEM of three biological replicates. **D.** PCA of RIC mass spectrometry data from all 3 WT and *vhl-1(ok161)* crosslinked and non-crosslinked samples including outliers. WT samples are indicated in red and *vhl-1(ok161)* in blue. Crosslinked samples are indicated by circles and non-crosslinked samples by squares. Excluded outliers are indicated by arrows. **E.-F.** Heat map showing the hierarchical clustering of all RIC replicates before (E) and after removal of two non-crosslinked samples (F) from WT and *vhl-1(ok161)* mutant, respectively. The iBAQ intensity range is indicated from 10 (blue) over 21 (white) to 32 (red).

Figure S2

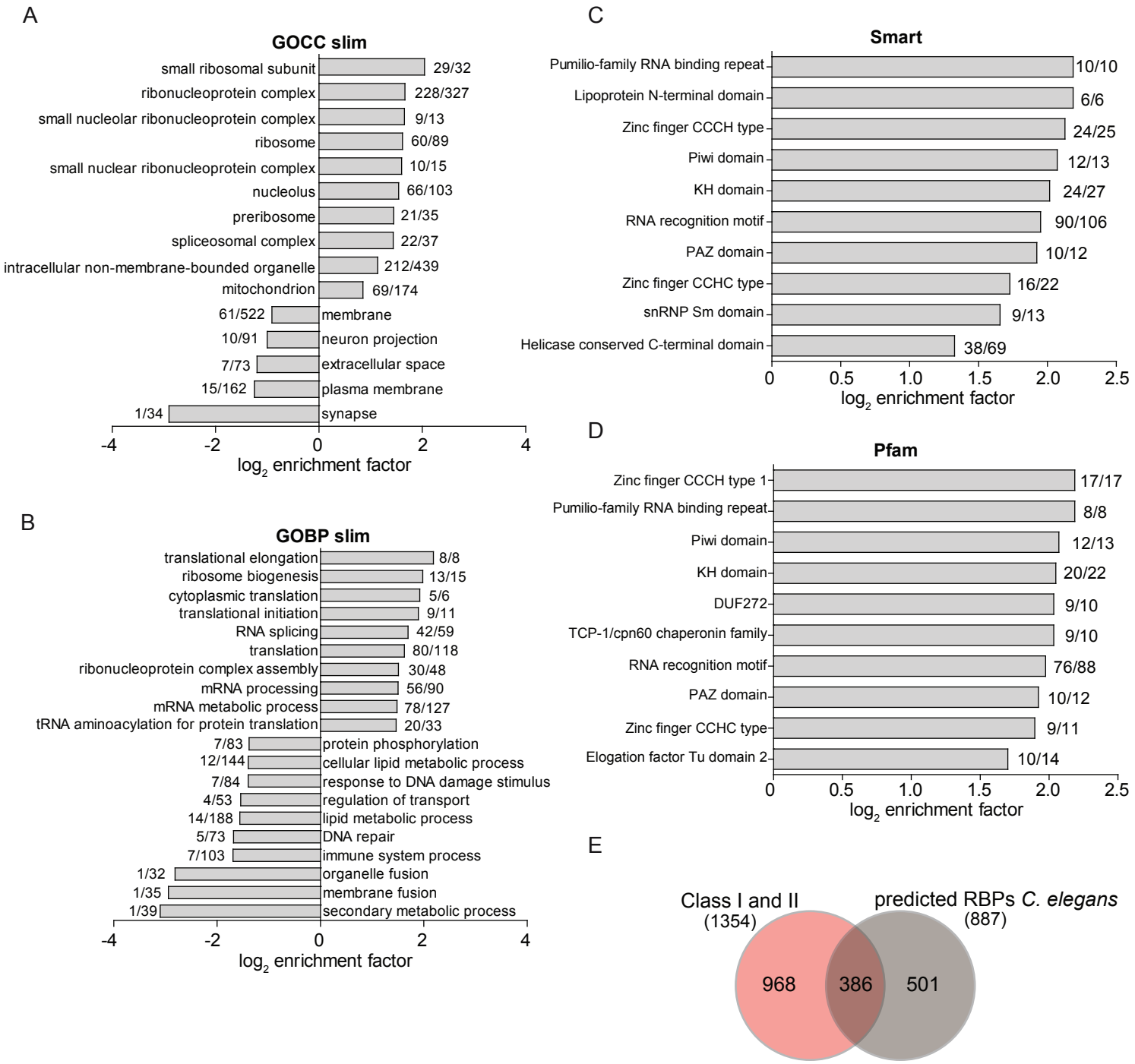
A
GOCC slim
small ribosomal subunit 29/32
ribonucleoprotein complex 228/327
small nucleolar ribonucleoprotein complex 9/13
ribosome 60/89
small nuclear ribonucleoprotein complex 10/15
nucleolus 66/103
preribosome 21/35
spliceosomal complex 22/37
intracellular non-membrane-bounded organelle 212/439
mitochondrion 69/174
61/522 membrane
10/91 neuron projection
7/73 extracellular space
15/162 plasma membrane
1/34 synapse
-4 -2 0 2 4
log2 enrichment factor
B
GOBP slim
translational elongation 8/8
ribosome biogenesis 13/15
cytoplasmic translation 5/6
translational initiation 9/11
RNA splicing 42/59
translation 80/118
ribonucleoprotein complex assembly 30/48
mRNA processing 56/90
mRNA metabolic process 78/127
tRNA aminoacylation for protein translation 20/33
7/83 protein phosphorylation
12/144 cellular lipid metabolic process
7/84 response to DNA damage stimulus
4/53 regulation of transport
14/188 lipid metabolic process
5/73 DNA repair
7/103 immune system process
1/32 organelle fusion
1/35 membrane fusion
1/39 secondary metabolic process
-4 -2 0 2 4
log2 enrichment factor
C
Smart
Pumilio-family RNA binding repeat 10/10
Lipoprotein N-terminal domain 6/6
Zinc finger CCCH type 24/25
Piwi domain 12/13
KH domain 24/27
RNA recognition motif 90/106
PAZ domain 10/12
Zinc finger CCHC type 16/22
snRNP Sm domain 9/13
Helicase conserved C-terminal domain 38/69
0 0.5 1.0 1.5 2.0 2.5
log2 enrichment factor
D
Pfam
Zinc finger CCCH type 1 17/17
Pumilio-family RNA binding repeat 8/8
Piwi domain 12/13
KH domain 20/22
DUF272 9/10
TCP-1/cpn60 chaperonin family 9/10
RNA recognition motif 76/88
PAZ domain 10/12
Zinc finger CCHC type 9/11
Elogation factor Tu domain 2 10/14
0 0.5 1.0 1.5 2.0 2.5
log2 enrichment factor
E
Class I and II
(1354)
predicted RBPs C. elegans
(887)
968
386
501

Figure S2. GO-term enrichment analysis of the *C. elegans* RIC dataset, Related to Figure 2

A. The enrichment analysis of gene ontology cellular compartments (GOCC) of the combined RBPome from WT and *vhl-1(ok161)* using the combined proteomes of WT and *vhl-1(ok161)* as background. Bar diagram depicting the top ten significant terms showing the highest and lowest enrichment factors (p-value<0.001). The number of proteins contained in the RBPome followed by category size is shown next to each bar. **B.** Bar diagram depicting the enrichment analysis of gene ontology biological processes (GOBP) (for diagram details see B.). **C.** SMART analyses of the combined RBPome from WT and *vhl-1(ok161)* using the combined proteomes of WT and *vhl-1(ok161)* as background. Bar diagram depicting the top ten overrepresented protein domains (p-value<0.001). The number of proteins contained in the RBPome followed by category size is shown next to each bar. **D.** Bar diagram depicting Pfam analyses (for diagram details see D.). **E.** Venn diagram showing the comparison of the combined Class I and II *C.elegans* RBPs from WT and *vhl-1(ok161)* to a list of predicted *C. elegans* RBPs (Tamburino et al., 2013).

Figure S3

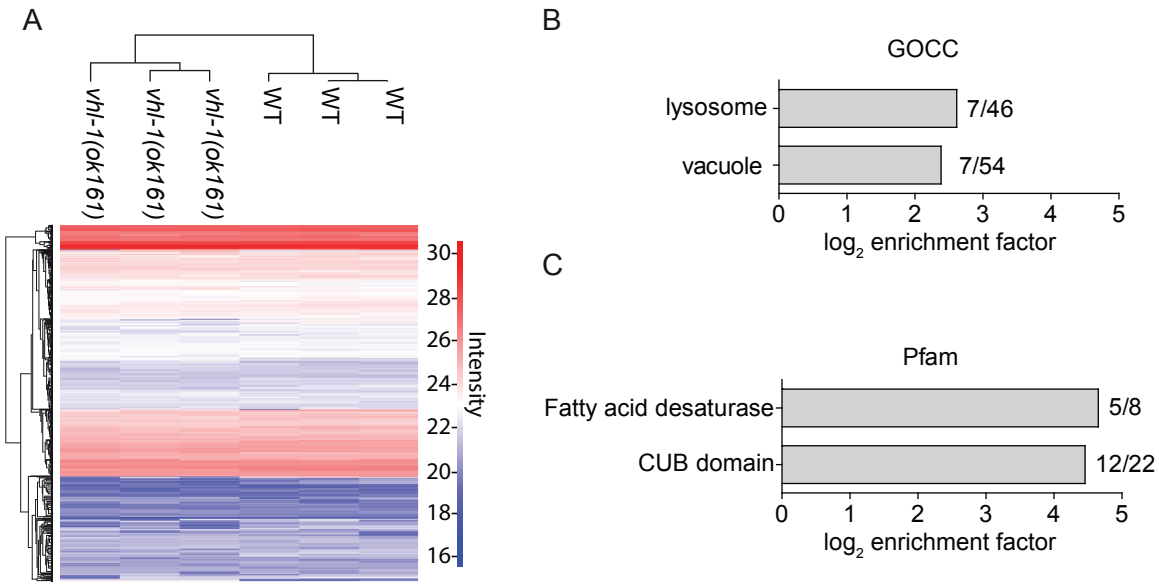
A
vhl-1(ok161)
vhl-1(ok161)
vhl-1(ok161)
WT
WT
WT
30
28
26
24
22
20
18
16
Intensity
B
GOCC
lysosome
7/46
vacuole
7/54
0
1
2
3
4
5
log2 enrichment factor
C
Pfam
Fatty acid desaturase
5/8
CUB domain
12/22
0
1
2
3
4
5
log2 enrichment factor

Figure S3. Analysis of the proteome of *vhl-1* mutant worms, Related to Figure 3

A. Heat map depicting the hierarchical clustering of all proteome replicates from WT and *vhl-1(ok161)* mutant samples. The iBAQ intensity range is indicated from 10 (blue) over 21 (white) to 32 (red). **B.** The enrichment analysis of gene ontology cellular compartments (GOCC) of the significantly regulated proteins in the proteome from WT and *vhl-1(ok161)* using the whole proteome as background. Bar diagram depicting the significantly enriched terms (p-value<0.001). The number of proteins contained in the proteome followed by category size is shown next to each bar. **C.** Pfam analyses of the significantly regulated proteins in the proteome from WT and *vhl-1(ok161)* using the whole proteome as background. Bar diagram depicting the top ten overrepresented protein domains (p-value<0.001). The number of proteins contained in the proteome followed by category size is shown next to each bar.

Figure S4

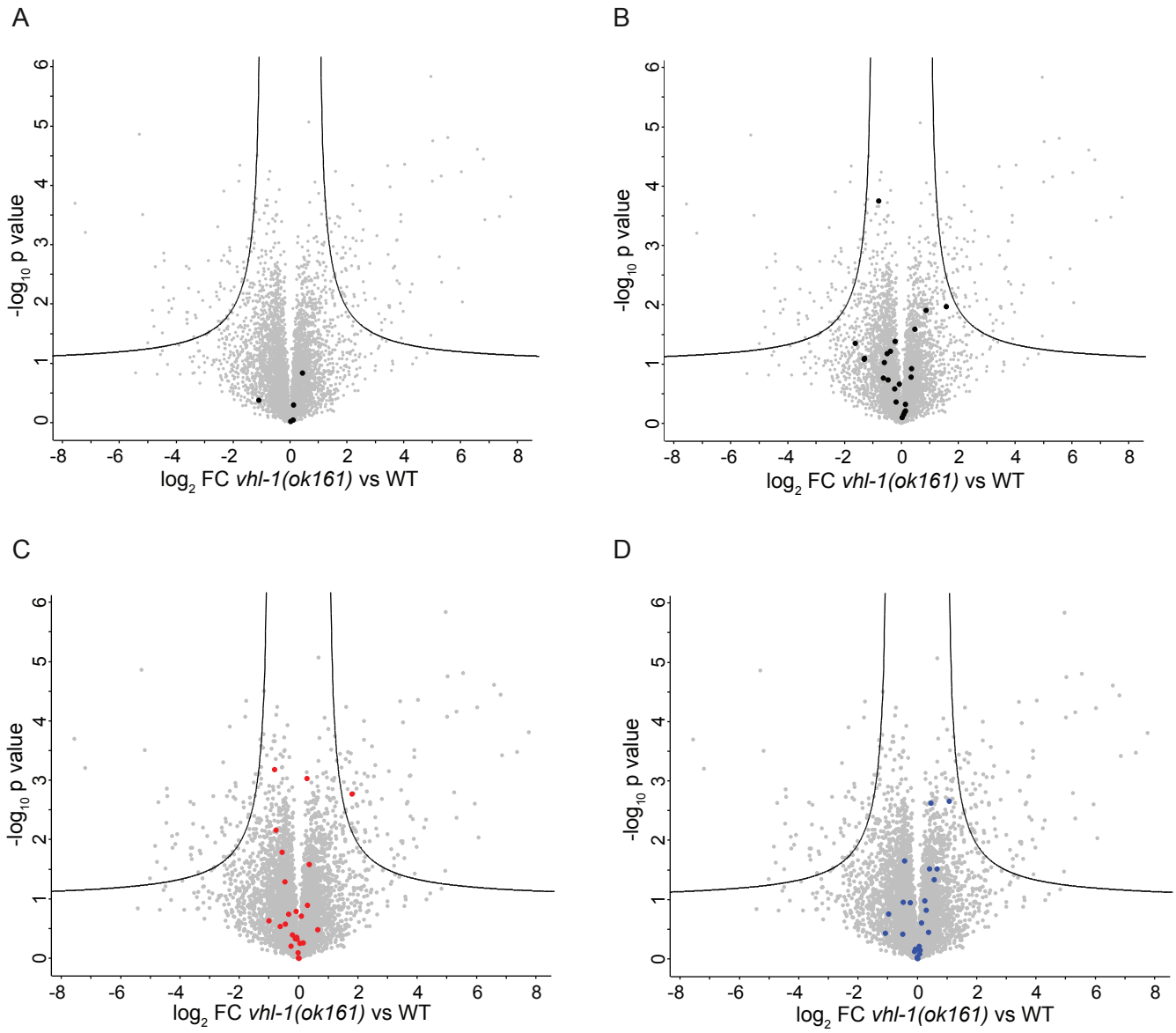
A
B
C
D
-log10 p value
log2 FC vhl-1(ok161) vs WT
0
1
2
3
4
5
6
-8
-6
-4
-2
0
2
4
6
8

Figure S4. Analysis of quantitative and qualitative changed RBPs in *vhl-1* mutant worms proteome, Related to Figure 4

Volcano plots illustrating the proteomes of *vhl-1(ok161)* and WT indicating no change of RBP abundance. The $-\log_{10}$ p-value is plotted against the $\log_2$ fold change (*vhl-1(ok161)* versus WT). Proteins above the black cutoff line are considered significant (FDR<0.05). In total, 5759 proteins were plotted. **A.** RBPs detected in all three crosslinked RIC samples of *vhl-1(ok161)* and never in WT are shown in black (for individual RBP information refer to Figure 4A). **B.** RBPs only detected in all three crosslinked RIC samples of WT and never in *vhl-1(ok161)* are shown in black (for individual RBP information refer to Figure 4B). **C.** RBPs enriched in WT RIC based on the prediction interval analysis presented in Figure 4C are highlighted in red. The only significant (FDR<0.05) protein was H28G03.1. **D.** Proteins enriched in *vhl-1(ok161)* RIC based on the prediction interval analysis presented in Figure 4C are highlighted in blue.

Transparent Methods

RESOURCES TABLE

REAGENT or RESOURCE	SOURCE	IDENTIFIER
Bacterial and Virus Strains		
Escherichia coli (OP50)	CGC	N/A
Chemicals, Peptides, and Recombinant Proteins		
Benzonase	Merck	Cat#70746
RNAse I	Thermo Fisher Scientific	Cat#AM2294
EDTA-free Protease Inhibitor Cocktail	Sigma-Aldrich	Cat#4693132001
Critical Commercial Assays		
Silver Stain Kit	Thermo Fisher Scientific	Cat#24612
Qubit RNA HS Assay Kit	Thermo Fisher Scientific	Cat#Q32852
Pierce™ BCA Protein Assay Kit	Thermo Fisher Scientific	Cat#23225
Deposited Data		
Analyzed data	This paper and Shiny app	https://kabo.shinyapps.io/celegans_rbpome/
Raw data and MaxQuant (version 1.5.3.8) output	PRIDE repository: PXD014469	http://www.ebi.ac.uk/pride
Experimental Models: Organisms/Strains		
C. elegans WT	CGC	N2
C. elegans *vhl-1(ok161)*	CGC	CB5602
Software and Algorithms		
MaxQuant (version 1.5.3.8)		https://www.maxquant.org/
Perseus software (version 1.6.2.2)	Tyanova et al., 2016	https://www.maxquant.org/perseus/
Prism (version 6)		https://www.graphpad.com/
Other		
Dynabeads Oligo(dT)25	Thermo Fisher Scientific	Cat#61002
4-12% Bis-Tris Protein Gels	Thermo Fisher Scientific	Cat#NP0321BOX
Tissue grinders 7ml, Tenbroeck type	VWR	CAT#432-1277

Strains

The worm strains N2 Bristol (WT) and seven times backcrossed *vhl-1*(ok161) (referred to as *vhl-1*) were used in this study. The worms were grown at 20°C on nematode growth medium (NGM) (WormBook), using standard techniques (Brenner, 1974). *E. coli* strain OP50 was used as a food source in all experiments. All worms and bacterial strains were provided by the *C. elegans* Genetics Center (CGC).

Sampling of *C. elegans* for RIC and Proteome

300.000 worms were grown for each replicate (3 for *vhl-1* and 3 for WT) in liquid culture using S medium (WormBook) and kept under shaking (110 rpm) at 20°C. After reaching young adult stage (about 72 hours after hatching), worms were harvested and washed three

times in M9 buffer (WormBook). After settling down in a 50 ml tube on ice, the supernatant was discarded and the worms were transferred to an empty NGM plate. Half of the worms (150.000) were irradiated with UV-C (254 nm) at 300mJ/cm² (Stratalinker 1800). Afterwards the worms were collected in M9 buffer and resuspended in lysis buffer (100 mM Tris pH 7.5, 500 mM LiCl, 10 mM EDTA pH 8, 1% LiDS, 5 mM DTT, protease inhibitor PIM). The non-crosslinked worms (150.000) were directly resuspended in lysis buffer. Worm lysates were prepared using a dounce homogenizer (Tissue grinders, Tenbroeck type) performing fifty strokes for each sample and checking at the stereomicroscope for complete homogenization. The lysates were directly used for RNA interactome capture and a fraction of the same lysate for proteome analysis.

RNA interactome capture (RIC)

RIC was performed as previously described (Ignarski et al., 2019) and adapted to *C. elegans*. Briefly, each worm lysates sample were incubated with 2 ml oligo(dT) magnetic beads (Thermo Fischer Scientific) rotating for 1 hour at 4°C. The beads were collected on a magnet and the supernatants were saved for two additional rounds of depletion. Beads were washed three times with 10 ml lysis buffer, three times with 10 ml washing buffer (50 mM Tris pH 7.5, 140 mM LiCl, 2 mM EDTA pH 8, 0.5% NP40) and once with 10 ml washing buffer without NP40. After the last wash the beads were resuspended in 300 µl elution buffer (10 mM Tris pH 7.5) and incubated at 80°C for 2 minutes. The protocol was repeated three times in total and the three eluted fractions were combined. An aliquot from each sample was taken and RNA concentration was measured using a Qubit™ RNA HS Assay Kit. To remove RNA before MS and silver gel analysis, the combined fractions were RNase digested (10 U/ml RNAse I, 125 U/ml Benzonase, 1 M $MgCl_2$) by incubation at 37°C for 3 hours. Two percent of the RNAse digested fraction were loaded on a SDS-PAGE gel (4-12%, Thermo Fischer Scientific) and stained by silver staining (Pierce™ Silver Stain Kit) for quality control.

Protein digestion

Protein digestion was performed according to a published protocol using carboxylate modified paramagnetic beads (Hughes et al., 2014) on the pooled eluate from crosslinked

and non-crosslinked samples of WT and *vhl-1(ok161)* and whole worm lysates of WT and *vhl-1(ok161)*. Briefly, samples were reduced in 5 mM dithiothreitol (DTT) incubating at 55°C for 30 min. Reduced cysteine residues were alkylated by adding chloroacetamide (CAA) to 40 mM for 30 min at room temperature in the dark. The samples were then centrifuged for 10 min at 20,000 x g and the supernatants were transferred to a new tube. Hydrophilic and hydrophobic Sera-Mag carboxylate-modified magnetic particles (GE Healthcare) were combined 1:1, washed two times with 10 volumes of water and resuspended at a concentration of 10 µg/µl with water. 2 µl of the bead mix were added to the samples and acetonitrile (ACN) was added to a final percentage of 50%. The mixture was incubated at room temperature for 8 min and placed on a magnetic rack for 2 min. Supernatants were removed and the beads were washed twice with 200 µl of 70% Ethanol (EtOH) and once with 100% ACN. The beads were air dried and reconstituted in 5 µl 50mM triethylammonium bicarbonate (TEAB) containing 0.5 µg trypsin and 0.5 µg LysC. Proteins were digested for 16 hours at 37°C. The beads were resuspended by pipetting up and down and ACN was added to 95 % final. The mixture was incubated at room temperature for 8 min and placed on a magnetic rack for 3 min. Supernatants were removed and the beads were washed twice with 200 µl of 100% ACN. Peptides were eluted from the beads by the addition 9 µl 4% dimethyl sulfoxide (DMSO) and sonication for 5 min. Samples were placed on a magnetic rack and the supernatants were transferred to new tubes. This step was repeated once to ensure complete removal of magnetic beads. Peptides were acidified by the addition of 1 µl 10% formic acid and stored at -20 °C until LC-MS analysis.

LC-MS Acquisition

All samples were analyzed on a Q Exactive Plus Orbitrap (Thermo Scientific) mass spectrometer that was coupled to an EASY nLC LC (Thermo Scientific). Peptides were loaded onto an in-house packed analytical column (50 cm — 75 µm I.D., filled with 2.7 µm Poroshell EC120 C18, Agilent) that was operated at a constant flowrate of 250 nl/min at 50°C. Depending on the experiment type, one of three different chromatographic gradients was used. 240 min: 4-5% solvent B (0.1% formic acid in 80% acetonitrile) within 1.0 min, 5-

28% solvent B within 200.0 min, 28-50% solvent B within 28.0 min, 50-95% solvent B within 1.0 min, 150 min: 3-5% solvent B (0.1% formic acid in 80% acetonitrile) within 1.0 min, 5-30% solvent B within 119.0 min, 30-50% solvent B within 19.0 min, 50-95% solvent B within 1.0 min 90 min: 3-5% solvent B (0.1% formic acid in 80% acetonitrile) within 1.0 min, 5-30% solvent B within 65.0 min, 30-50% solvent B within 13.0 min, 50-95% solvent B within 1.0 min. All gradients included final wash and column equilibration steps. Depending on gradient length, peptide precursors were dynamically excluded for 40.0 s, 25 s or 15 sec. MS1 survey scans were acquired from 300-1750 m/z at a resolution of 70,000. The top 10 most abundant peptides were isolated within a 1.8 Th window and subjected to HCD fragmentation at normalized collision energy of 27%. The AGC target was set to 5e5 charges, allowing maximum injection times of 60 ms (240 min and 150 min gradients) or 100 ms (90 min gradient). Product ions were detected in the Orbitrap at a resolution of 17,500.

Data analysis and statistics

Protein identification: All mass spectrometric raw data were processed with MaxQuant (version 1.5.3.8) using default parameters. Briefly, MS2 spectra were searched against the Uniprot CAEEL.fasta database (downloaded the 16.6.2017), including a list of common contaminants. False discovery rates on protein and PSM level were estimated by the target-decoy approach to 1% (Protein FDR) and 1% (PSM FDR) respectively. The minimal peptide length was set to 7 amino acids and carbamidomethylation at cysteine residues was considered as a fixed modification. Oxidation (M) and Acetyl (Protein N-term) were included as variable modifications. The match-between runs option was enabled.

Statistical analysis of both the whole proteome and the RNA interactome raw data was performed with the Perseus software (Tyanova et al., 2016), version 1.6.2.2. iBAQ intensities were used in this analysis and $\log_2$ transformed.

RNA interactome: Two samples (indicated by an arrow in S1 D) were identified as outliers based on the number of proteins measured, which were higher than in crosslinked samples and the results of PCA and hierarchical clustering (Figure S1D/E), Indicating that these samples possibly contaminated during processing e.g. with the whole worm lysates and

therefore excluded from further analyses (see also “Limitations of the study”). T-test was performed for *vhl-1* crosslinked (n=3) versus non-crosslinked samples (n=2) and WT crosslinked (n=3) versus non-crosslinked samples (n=2) using FDR<0.05 and s0=0.5.

Whole Proteome: After filtering for proteins measured at least 3 times out of 6 replicates in total (WT and *vhl-1*) the median was subtracted and x+(highest median)+1 was added, missing values were imputed by replacing missing values from normal distribution (width 0.3, down shift 1.8) and significantly regulated proteins were identified using a t-test (FDR<0.05, s0=0.5).

Categorical annotation and enrichment analysis: The uniprot IDs were annotated using Perseus software for Gene ontology (GO), PFAM, SMART and KEGG. Gene set enrichment analysis of the combined Class I and II RIC of *vhl-1* and WT was calculated using a Fisher exact test (Perseus standard settings, FDR<0.05 (Tyanova et al., 2016)), and the total number of proteins identified in both RIC and Protome MS experiments was used as a background.

Correlation analysis WT vs. *vhl-1* RNA interactome: The linear regression of $\log_2$ fold change of WT versus *vhl-1* was calculated with R (version 3.4.4) using the method *deming()* from the R package *deming* (version 1.4 (https://cran.r-project.org/web/packages/deming/index.html)) which applies the method of total least squares. This results in the formula y = 0.7806137 + 1.095646*x with $\log_2$ fold change of *vhl-1* on x-axis and values of WT on y-axis. To get the proteins that are more enriched in *vhl-1* or WT, we calculated the linear equations that define the upper and lower boundary of the interval in which 95% of all measurements lie, in other words the 95% prediction interval. This interval is defined by multiplying the standard deviation of the regression (1.562865) by 1.96 and adding or subtracting this value to the intercept of the regression line for the upper and lower boundary, respectively. The linear equation for the upper boundary is y = 3.843829 + 1.095646*x, the equation for the lower boundary is y = -2.282602 + 1.095646*x.

Data and Software Availability

The mass spectrometry data (Raw data and MaxQuant (version 1.5.3.8) output) have been deposited to the ProteomeXchange Consortium (http://www.ebi.ac.uk/pride) via the PRIDE (Perez-Riverol et al., 2019) partner repository with the dataset identifier PXD014469.

An interactive online repository was created and is provided at http://shiny.cecad.uni-koeln.de:3838/celegans_rbpome.

References

Brenner, S. (1974). The genetics of Caenorhabditis elegans. Genetics 77, 71-94. https://cran.r-project.org/web/packages/deming/index.html.

Hughes, C.S., Foehr, S., Garfield, D.A., Furlong, E.E., Steinmetz, L.M., and Krijgsveld, J. (2014). Ultrasensitive proteome analysis using paramagnetic bead technology. Mol Syst Biol 10, 757.

Ignarski, M., Rill, C., Kaiser, R.W.J., Kaldirim, M., Neuhaus, R., Esmaillie, R., Li, X., Klein, C., Bohl, K., Petersen, M., et al. (2019). The RNA-Protein Interactome of Differentiated Kidney Tubular Epithelial Cells. J Am Soc Nephrol.

Perez-Riverol, Y., Csordas, A., Bai, J., Bernal-Llinares, M., Hewapathirana, S., Kundu, D.J., Inuganti, A., Griss, J., Mayer, G., Eisenacher, M., et al. (2019). The PRIDE database and related tools and resources in 2019: improving support for quantification data. Nucleic Acids Res 47, D442-d450.

Tamburino, A.M., Ryder, S.P., and Walhout, A.J. (2013). A compendium of Caenorhabditis elegans RNA binding proteins predicts extensive regulation at multiple levels. G3 (Bethesda) 3, 297-304.

Tyanova, S., Temu, T., Sinitcyn, P., Carlson, A., Hein, M.Y., Geiger, T., Mann, M., and Cox, J. (2016). The Perseus computational platform for comprehensive analysis of (prote)omics data. Nat Methods 13, 731-740.

WormBook. Maintenance of C. elegans (http://www.wormbook.org/chapters/www_strainmaintain/strainmaintain.html).